Ions, after acceleration, drift in 63mm long field free region and are detected by a channeltron. A second detector, again a channeltron, placed very close to the ionisation region, but on the opposite side of the ion flight tube, is used to detect electrons. Both detectors are operated in the particle counting mode. Signals from the two detectors are processed by fast amplifiers followed by constant fraction discriminator. Time-of-flight measurement is done by using the electron detector signal as the start pulse and ion detector signal as the stop pulse. The time difference between the start and stop pulse gives the information about the flight time and thus the charge state of the produced ions. Although the photon beam is pulsed, its repetition rate is too high to be useful for ion flight time measurement.

Gas pressure is monitored using a capacitance manometer. Measuring the current from a photodiode monitors the photon flux. For comparing ion yields at different photon energies, the ion yield for each charge state is normalised to the integrated photon flux and gas flow rate. Data acquisition and control is developed on a LABVIEW platform.

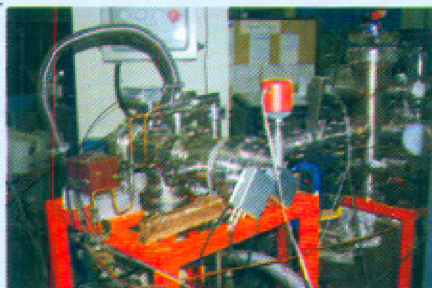

Fig. A.11.2 TOP Experimental station on CAT TGM beamline

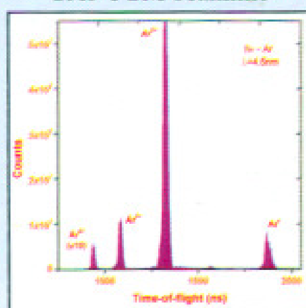

Fig. A.11.3 TIOF Spectrum of photoionized argon

We are currently studying multiple ionization of argon. Significant changes in the yield of different calibration charge states are observed around the argon L edge (245eV). Charge states upto Ar^{4+} have been identified (fig.A.11.3). This work was done in collaboration with a team from PRL, Ahmedabad.

(Contributed by: B. Bapat, R K Singh, K P Subramanian, G S Lodha; lodha@cat.ernet.in)

A.12 Valence bands offset measurement between two semiconductors using Indus-1

A modified method has been used to measure the valence bands offset by photoelectron spectroscopy (PES) between low doped and depleted semiconductors. PES measurements have been done on the angle resolved photoemission spectroscopy beam line of Indus-1 synchrotron radiation source. The valence bands offset at the heterojunction of depleted ZnSe film and doped GaAs substrate have been measured. ZnSe films were deposited on doped GaAs substrates by the laser ablation technique. The surface photovoltage (SPV) and the charging effects modify the PES spectra of depleted semiconductors. The shift of PES spectra of ZnSe film by about 6eV has been observed due to the charging and SPV effects. The charging and SPV effects on PES spectra have been reduced to negligible values in the presence of excess plasma density (due to absorption of white light from a tungsten lamp (the secondary source) of the order of $10^{18}cm^{-3}$.

In figure A.12.1, shifts of PES spectra of 1μm thick ZnSe film, sample1, are shown in the presence of increasing secondary photon fluxes. Curve 1 is in the dark background (i.e. tungsten lamp was off). Secondary photon fluxes for curves 2, 3 and 4 are about $9x10^{11}cm^{-2}sec^{-1}$, $1.2x\ 10^{12}cm^{-2}sec^{-1}$ and $5x10^{12}cm^{-2}sec^{-1}$ respectively. The inset shows the shift of the Zn-3d peak as a function of the secondary photon fluxes. The energy of the primary beam was 154eV and the photon flux for all the curves was in the range of $2\text{-}5x10^{11}cm^{-2}sec^{-1}$. In figure A.12.2, PES spectra of ZnSe film of thickness 0.2μm are shown. Curves 1 and 2 are in the dark background and in the presence of the secondary photon flux $5x10^{12}cm^{-2}sec^{-1}$ respectively. The energy of the primary beam was 130eV and the photon flux for all the curves was in the range of $2\text{-}5x10^{11}\ cm^{-2}sec^{-1}$. These results clearly show that the effect of the charging and SPV are different for two samples. The PES spectra measured in the presence of the excess plasma density ($\approx 5x10^{18}cm^{-3}$) have been used to measure the valence band onset energies of GaAs and ZnSe and the core level energies of Ga-3d and Zn-3d. These values of valence band onset energies and core level energies have been used to calculate the valence bands offset between ZnSe and GaAs and it is found to be $1.1\pm0.1eV$.

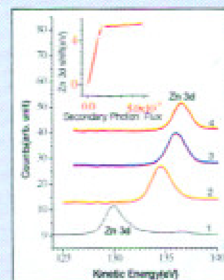

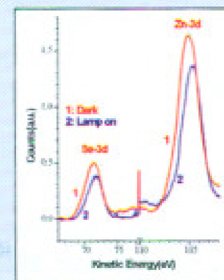

Fig. A.12.1 **Fig. A.12.2**

This value of valence bands offset matches with the published values for samples prepared in the in-situ conditions. The importance of the present method is that it is useful for samples prepared in ex-situ conditions with film thickness of the order of 100nm. This work was done in collaboration with a team from BARC.

(Contributed by: Shailendra Kumar, S.N. Jha, Jagannath, Tapas Ganguly, S.V.N. Bhaskara Rao, N.C. Das; shail@cat.ernet.in)

A.13 W/C X-ray multilayer mirror

X-ray multilayer devices consist of periodic arrangement of alternating layers of two different materials. The reflections of incident wave field from the successive interfaces in the multilayer add in phase at the Bragg condition and gives enhanced peak reflectivity. Smooth interfaces with chemical stability between the concerned materials are important prerequisites for making an ideal device. In x-ray mirrors, the interface roughness severely degrades the optics quality. Shape of the interfaces and their correlations and conformity with underneath layers are among the most important parameters. We have studied a W/C multilayer (C ~70Å/W ~40Å) by hard and soft x-ray reflectivity measurements. The hard x-ray reflectivity measurements are carried out using CuKα radiation (λ=1.54Å) and soft x-ray reflectivity measurement at λ=80Å using Indus-1 (fig. A.13.1 and fig. A.13.2). Detailed analysis of reflectivity data reveals that, in W/C multilayer, the roughness propagates across the successive layers from bottom to top layer. It is found that the roughness propagation factors for the two types of interfaces viz. W-on-C interface and C-on-W interface are different. In case of W-on-C interface the roughness propagation is slower in comparison to C-on-W interface. Amorphous carbon, which acts as a roughness suppresser, is responsible for asymmetric interface behavior. In fig.A.13.1 the best fit represented by continuous line is obtained by accumulated roughness model. The same model has been applied for the soft x-ray measurement and results are found in good agreement with hard x-ray data.

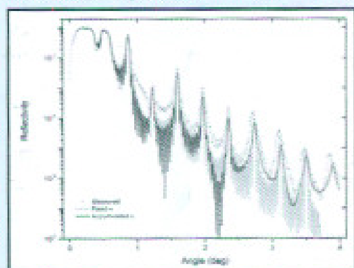

Fig. A.13.1 X-ray reflectivity spectra of W/C multilayer using λ=1.54Å wavelength is shown *along with the fitted curve*

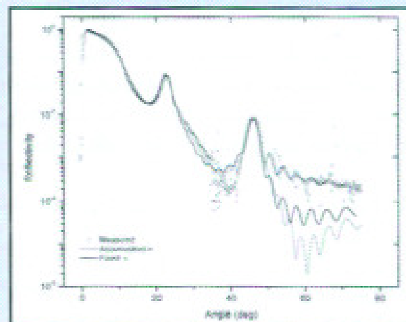

Fig A.13.2 X-ray reflectivity spectra of W/C multilayer at λ=80Å with the fitted curve.

(Contributed by: Dr. GS Lodha; lodha@cat.ernet.in))

A.14 Use of DC accelerator for radiation processing

A 750kV, 20kW DC electron accelerator designed and built at CAT, is currently being used to develop various processes relating to radiation processing of materials and food items. The beam from this electron accelerator provides an irradiation span 1.2 meters wide and (at 400keV) can penetrate 2mm deep in unit density material. The complete system is installed in a shielded area and is at present operating at 2.5kW power level, as permitted by the Atomic Energy Regulatory Board.

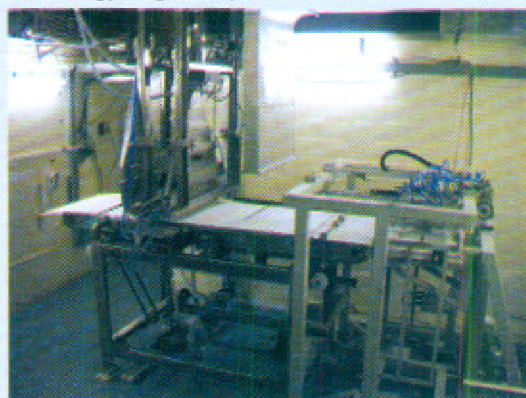

Fig.A.14.1 Irradiation of paper

Fig. A.14.2 Irradiation of wood